A new water retention model considering pore non-uniformity and evolution of pore size distribution

Authors: Q. Cheng, C. W. W. Ng, C. Zhou* and C. S. Tang

*Corresponding author

Information of the authors

First author: Dr Q. Cheng

Assistant Researcher, School of Earth Sciences and Engineering, Nanjing University, Nanjing, Jiangsu Province, China

E-mail: qcheng@connect.ust.hk

Co-author: Prof. C. W. W. Ng

CLP Holdings Professor of Sustainability, Department of Civil and Environmental Engineering, the Hong Kong University of Science and Technology, Kowloon, Hong Kong

E-mail: cecwwng@ust.hk

Co-author: Dr C. Zhou

Assistant Professor, Department of Civil and Environmental Engineering, the Hong Kong Polytechnic University, Hung Hom, Kowloon, Hong Kong

E-mail: c.zhou@polyu.edu.hk

Co-author: Prof C. S. Tang

Professor, School of Earth Sciences and Engineering, Nanjing University, Nanjing, Jiangsu Province, China

E-mail: tangchaosheng@nju.edu.cn

Abstract

Pore size distribution (PSD), which is usually measured through mercury intrusion porosimetry (MIP) tests, is often used to predict the water retention curve (WRC) of unsaturated soil. Existing models generally predict the drying path of the WRC only, because the intrusion of non-wetting mercury in MIP tests is equivalent to air entry during drying. Moreover, the PSD changes under hydro-mechanical loads, which has a significant influence on water retention behaviour. In this study, a new model is developed to predict both the main drying and wetting paths of WRCs. Based on a single PSD at reference stress and suction conditions, the influence of pore non-uniformity on MIP test results and the main drying and wetting paths of WRCs is quantified by the new model. From the reference PSD, the variation in the PSD with stress and suction is determined and incorporated in modelling the WRC. The newly developed model is applied to simulate the PSD variation and the hysteretic WRC of different soils. It is evident that the new model is able to capture the evolution of the PSD during drying, wetting and compression. Moreover, the main drying and wetting paths of WRCs of unsaturated soil are closely predicted.

Keywords: water retention; pore size distribution; non-uniformity; main drying and wetting

Introduction

Water retention characteristics is an essential property of unsaturated soil in geotechnical engineering (Ng and Menzies, 2007; Dolinar, 2015). Experimentally measuring the water retention curve (WRC) of unsaturated soil takes up to several months (Vanapalli et al., 1999; Puppala et al., 2006; Ng et al., 2012; Satyanaga et al., 2013). As water retention behaviour is mainly governed by the pore size distribution (PSD) (Ng and Pang, 2000; Zhou and Ng, 2014), it is reasonable to deduce the WRC using mercury intrusion porosimetry (MIP). However, existing models can only predict the drying path of the WRC. This limitation is mainly due to the fact that the PSD obtained from MIP tests does not represent the intrinsic PSD of soil because of the influence of pore non-uniformity (Hillel, 1998). Pore non-uniformity means that in the pore network architecture, a soil pore with a given radius is bounded by larger or smaller pores. In this study, the intrinsic PSD is the PSD without the influence of pore non-uniformity. It is not identical as the measure one. Moreover, the process of non-wetting mercury intruding into soil pores in MIP tests is equivalent to the entry of non-wetting air along the drying path (Romero and Simms, 2008). Hence, the WRC predicted from MIP results corresponds to the drying path. To predict the wetting path of the WRC, further study is required to quantify the influence of pore non-uniformity on MIP results and water retention behaviour.

Another limitation of most existing models, which directly predict the WRC from the PSD, is the assumption of a constant PSD (Prapaharan et al., 1985; Romero et al., 1999; Zhang and Li, 2010; Sun et al., 2016). This assumption is inconsistent with many experimental results reported in the literature, which shows that the PSD of unsaturated soil changes with stress and suction (Simms and Yanful, 2001; Li and Zhang, 2009; Nowamooz and Masrouri, 2010; Yu et al., 2016; Gao et al., 2018). Moreover, Zhou and Ng (2014) illustrated that the prediction errors of WRC models that ignore changes in the PSD are non-negligible.

In this study, a new model is developed to predict both the main drying and wetting paths of the WRC. The effects of pore non-uniformity and change in PSD are incorporated. The newly developed model is applied to simulate the PSD and WRC of different soils for verification. Measured and computed results are compared and analysed.

Effects of pore non-uniformity on water retention during drying and wetting

According to the Young-Laplace equation (Ng and Menzies, 2007), the relationship between matric suction s and pore radius r is described by

$$s = \frac{2T_S \cos\theta}{r}, \quad (1)$$

where s is matric suction (kPa), which is defined as the difference between the pore air pressure (u_a) and the pore water pressure (u_w) acting on the air-water interface; T_s is the surface tension of water, which is equal to 72.8 mN/m at 20°C; and θ is the contact angle (°) between the air-water interface and the soil particle.

Equation (1) can be used to describe the water retention behaviour of soil pores. Assuming that the radius of a pore is uniform, water drains from larger pores first during the drying process. During the wetting process, water tends to fill smaller pores first. Fig. 1(a) shows an idealised pore PA with a uniform radius of r_0. During the drying process, when suction increases to $2T_s \cos\theta/r_0$, water drains from PA. During the wetting process, when suction decreases to $2T_s \cos\theta/r_0$, water enters and fills PA. Note that Fig. 1(a) does not account for pore non-uniformity, which is in fact very common and affects water retention during drying and wetting processes (Hillel, 1998). For instance, Fig. 1(b) shows a given pore PA with a radius of r_0 bounded by larger pores PB with a radius of R ($R > r_0$). Fig. 1(c) shows another example, in which a given pore PA with a radius of r_0 is bounded by smaller pores PC with a radius of r' ($r' < r_0$). The pore non-uniformity has a significant influence on the water retention behaviour of unsaturated soil (Hillel, 1998). Similarly, due to its influence on mercury intrusion (Penumadu and Dean, 2000), the PSD obtained from MIP tests does not represent the intrinsic PSD of soil. The influence of pore non-uniformity on the PSD and WRC is modelled in the following section.

Development of a new hysteretic water retention model

The following proposed model makes several assumptions. Soil is uniform and soil pores are idealised as parallel cylindrical bundles of tubes and the shape, size and cross-section of each tube remain constant along the length of the tube. The contact angle is assumed to be 0°. Hysteresis in the main drying and wetting paths is considered by taking the effects of pore non-uniformity into account. However, hysteresis induced by the variation in contact angle is ignored.

Modelling the variation in the PSD under hydro-mechanical loads

The PSD of soil is often described by the pore volume density function $f(log(r))$, which is defined as follows (Fredlund and Xing, 1994):

$$f(log(r)) = \frac{d\theta_w}{d\,log(r)}, \quad (2)$$

where θ_w is the volumetric water content when all pores with a radius less than or equal to r are filled with water. Under hydro-mechanical loading, the PSD changes (Simms and Yanful, 2002; Nowamooz and Masrouri, 2010; Yu et al., 2016; Gao et al., 2018). A simplified method for describing the shift of the PSD curve (modified from Hu et al., 2013) is shown in Fig. 2. The overall shape of the PSD curve after volume change is assumed to be the same as that in the initial state. In other words, the pore volume density at each pore radius changes together under hydro-mechanical loading. Two parameters are used to describe the variation in the PSD. One is the shifting factor controlling the parallel shift of the PSD curve along the horizontal axis. The other one is the scaling factor controlling the scale-up and scale-down of the pore volume density. When the soil volume expands, the initial PSD curve shifts towards the direction of a larger pore radius and a larger pore volume density at the same time. When the soil volume contracts, the initial PSD curve moves towards the direction of a smaller pore radius and a smaller pore volume density. The variation in the PSD can be described by the following equation:

$$f_i(log(r)) = \beta f_0(log(r) - log(\chi)), \quad (3)$$

where $f_0(log(r))$ is the pore volume density function in the initial state; $f_i(log(r))$ is the pore volume density function after hydro-mechanical loading; β is the scaling factor and χ is the shifting factor. When the PSD curve shifts towards the direction of a larger pore radius and a larger pore volume density under certain hydro-mechanical loading, β and χ increase. When the PSD curve shifts towards the direction of a smaller pore radius and a smaller pore volume density, β and χ decrease. The PSD curve is plotted in the $d\theta_w/dlog(r)$- $log(r)$ plane. A linear transformation and a constant scaling factor applied to the logarithm of the pore radius leads to the larger pores being more strongly affected than the smaller ones. This is supported by experimental evidence provided in previous studies (Romero et al., 2011; Burton et al., 2015; Yu et al., 2016; Li et al., 2018).

The shifting factor χ can be calibrated using the change in the mean pore radius r_p. By analysing a large set of published MIP data, Santamarina and Jang (2011) found that there is a relationship between

the mean pore radius r_p and the void ratio e as shown in Equation (4).

$$log(r_p) = \frac{k}{2S_s\rho}e, \tag{4}$$

where k is the shape factor describing different particle configurations; S_s is the specific surface (m^2); and ρ is the mineral density (kg/m^3). All three parameters are generally constant. Thus, Equation (4) can be simplified to

$$log(r_p) = Ke, \tag{5}$$

where K is a material parameter representing the relationship between the mean pore radius and the void ratio in the $log(r_p) - e$ plane. The relationship between the change in the mean pore radius and the variation in the void ratio can then be expressed as

$$log(r_{pi}) - log(r_{p0}) = K(e_i - e_0), \tag{6}$$

where r_{p0} is the mean pore radius in the initial state (μm); e_0 is the initial void ratio; e_i is the void ratio after hydro-mechanical loading and r_{pi} is the mean pore radius after hydro-mechanical loading (μm). It is assumed that the change in the radius of each pore is isometric and contributes to the macroscopic soil volume change (Simms and Yanful, 2005). According to Equations (3) and (6), the shifting factor χ can be determined as follows:

$$\chi = 10^{K(e_0 - e_i)} \tag{7}$$

The scaling factor β can be calibrated using the change in the saturated volumetric water content $\theta_{w,sat}$. In the initial state, the saturated volumetric water content $\theta_{w0,sat}$ of the soil specimen is expressed as

$$\theta_{w0,sat} = \int_{log(r_{min})}^{log(r_{\max})} f_0(log(r))d\,log(r). \tag{8}$$

After hydro-mechanical loading, the saturated volumetric water content $\theta_{wi,sat}$ of the soil specimen is expressed as

$$\theta_{wi,sat} = \int_{log(r_{min})}^{log(r_{\max})} \beta f_0(log(r) + log(\chi))d\,log(r). \tag{9}$$

Then, based on Equations (8) and (9), the scaling factor β can be determined as follows:

$$\beta = \frac{e_i(1+e_0)}{e_0(1+e_i)} \tag{10}$$

According to the elasto-plastic model for unsaturated soil (e.g. Alonso et al., 1990), a change in the void ratio can be induced by a change in net mean stress and a change in suction. The following equation

is used:

$$de = -\alpha_p \frac{dp}{p_r+p} - \alpha_s \frac{ds}{p_{atm}+s}, \quad (11)$$

where α_p and α_s represent soil compressibility with respect to the net mean stress and suction, respectively; p is the net mean stress (kPa); and p_r is a reference pressure (taken as 1 kPa). Atmospheric pressure decreases with increasing temperature as the air density drops. In this equation, p_{atm} is the standard atmospheric pressure (101 kPa at 0°C). Equation (11) is simplified and widely used in many elasto-plastic models to calculate the deformation of unsaturated soil (e.g. Alonso et al., 1990; Zhou and Ng, 2014). On the right-hand side, the two terms $\alpha_p \frac{dp}{p_r+p}$ and $\alpha_s \frac{ds}{p_{atm}+s}$ represent soil volume changes induced by a change in net mean stress and a change in suction, respectively. In this equation, shearing-induced volume change is not considered. The two parameters α_p and α_s are dependent on the yield surface and stress state. When the stress state is on the yield surface, the soil specimen is regarded as normally consolidated. For normally consolidated soil, α_p and α_s are equal to plastic compressibility indices λ_p and λ_s. When the stress state is inside the yield surface, the soil specimen is overly consolidated. To calculate elasto-plastic soil deformation, α_p and α_s are equated to elastic compressibility indices κ_p and κ_s. The void ratio *e* in Equation (11) takes the differential form. By integrating Equation (11), it can be found that the void ratio is equal to

$$e_i = e_0 - \alpha_p \, ln\left(1 + \frac{p_i}{p_r}\right) - \alpha_s \, ln\left(1 + \frac{s_i}{p_{atm}}\right), \quad (12)$$

where p_i is applied stress (kPa) and s_i is applied suction (kPa). By substituting Equation (12) into Equation (7), the shifting factor χ is determined by the following equation:

$$\chi = 10^{K\times\left(\alpha_p \, ln\left(1+\frac{p_i}{p_r}\right)+\alpha_s \, ln\left(1+\frac{s_i}{p_{atm}}\right)\right)} \quad (13)$$

Similarly, by substituting Equation (12) into Equation (10), the scaling factor β is determined as follows:

$$\beta = \frac{\left[e_0-\alpha_p \, ln\left(1+\frac{p_i}{p_r}\right)-\alpha_s \, ln\left(1+\frac{s_i}{p_{atm}}\right)\right](1+e_0)}{e_0\left[1+e_0-\alpha_p \, ln\left(1+\frac{p_i}{p_r}\right)-\alpha_s \, ln\left(1+\frac{s_i}{p_{atm}}\right)\right]} \quad (14)$$

Based on Equations (3), (13) and (14), the relationship between PSD variation and stress and suction can be calculated. By using these equations, a series of PSD curves during mechanical and hydraulic loading can be calculated from one measured PSD curve.

Deducing the intrinsic PSD from MIP test results

During drying, the amount of water θ_i drained from the pores with a radius larger than or equal to a given pore radius r^* can be expressed as

$$\theta_i = \int_{log(r^*)}^{log(r_{max})} f(log(r)) d\, log(r). \quad (15)$$

As discussed above, the process of mercury intruding into soil pores in MIP tests is influenced by pore non-uniformity (Penumadu and Dean, 2000). Thus, the measured PSD is already influenced by pore non-uniformity and is not the intrinsic PSD of the soil specimen. $F(log(r))$ is used to represent the pore volume density function of the intrinsic PSD. If there is no influence of pore non-uniformity, the amount of water θ_i' drained from the pores with a radius larger than or equal to r^* would be

$$\theta_i' = \int_{log(r^*)}^{log(r_{max})} F(log(r)) d\, log(r). \quad (16)$$

During drying, for the soil pore with a radius larger than or equal to r^* bounded by smaller pores, water inside cannot be drained at the corresponding suction as discussed before. For soil pores smaller than r^*, the fraction of the total porosity is

$$P_r = \int_{log(r_{min})}^{log(r^*)} F(log(r)) d\, log(r) \Big/ \int_{log(r_{min})}^{log(r_{max})} F(log(r)) d\, log(r). \quad (17)$$

Hence, the soil pores larger than r^* have a fraction of $(1 - P_r)$. During drying, water in some larger pores cannot be drained out at a suction of $(2T_s/r^*)$ since they are bounded by smaller pores. For this part of larger pores, the fraction of total porosity is

$$a = (1 - P_r)P_r^n, \quad (18)$$

where n equals to the number of pores to which an individual pore is connected. It is a variable dependent on pore lattice in the soil specimen. In this study, to minimize the number of model parameters, a cubic lattice is assumed for simplicity with n = 6. The relationship between θ_i and θ_i' is expressed as

$$\theta_i = \theta_i' - a \int_{log(r_{min})}^{log(r_{max})} F(log(r)) d\, log(r). \quad (19)$$

By combining Equations (15)-(19), the relationship between the measured pore volume density function $f(log(r))$ and the intrinsic one $F(log(r))$ can be obtained as follows:

$$\int_{log(r^*)}^{log(r_{max})} f(log(r))d\,log(r)$$

$$= \int_{log(r^*)}^{log(r_{max})} F(log(r))d\,log(r)\left[1-\left(\frac{\int_{log(r_{min})}^{log(r^*)} F(log(r))d\,log(r)}{\int_{log(r_{min})}^{log(r_{max})} F(log(r))d\,log(r)}\right)^n\right] \tag{20}$$

Using Equation (20), the intrinsic PSD without the influence of pore non-uniformity can be calculated.

Modelling the drying and wetting paths of the WRC

Based on the equations discussed in the previous sections, each intrinsic PSD not influenced by pore non-uniformity under a certain hydro-mechanical loading can be obtained. The volumetric water content θ_w when all pores with a radius smaller than or equal to r^* are filled with water can be calculated through the following equation:

$$\theta_w(log(r)) = \int_{log(r_{\min})}^{log(r^*)} F(log(r))d\,log(r) \tag{21}$$

Combining Equations (1) and (16) yields the relationship between the volumetric water content θ_w and suction s:

$$\theta_w(log(s)) = \int_{log(s^*)}^{log(s_{max})} G(log(s))d\,log(s), \tag{22}$$

where s_{max} is the maximum suction (kPa) corresponding to the minimum pore radius ($2T_s\,cos\,\theta/r_{min}$), $s^*$is the suction (kPa) corresponding to the given pore radius ($2T_s\,cos\,\theta/r^*$) and $G(log(s))$ is the pore capillary pressure distribution function ($d\theta_w/d\,log(s)$).

At a given suction s during the drying process, water in soil pores may be considered as consisting of two parts. The first part is the water in the soil pores with a radius equal to or smaller than the corresponding radius ($2T_s\,cos\,\theta/s^*$). The volumetric water content of this part can be expressed as

$$\theta_{wd1}(log(s)) = \int_{log(s^*)}^{log(s_{max})} G(log(s))d\,log(s). \tag{23}$$

The other part is the water in the soil pores bounded by smaller pores that cannot be drained because they are surrounded by smaller pores. The volume fraction of pores with a radius larger than or equal to r bounded by smaller pores b is represented as

$$b = \left(\int_{log(s^*)}^{log(s_{max})} G(log(s))d\,log(s)/\int_{log(s_{min})}^{log(s_{max})} G(log(s))d\,log(s)\right)^n. \tag{24}$$

Thus, the volumetric water content of the second part can be expressed as

$$\theta_{wd2}(log(s)) = b\int_{log(s_{min})}^{log(s^*)} G(log(s))d\,log(s). \quad (25)$$

By summing $\theta_{wd1}(log(s))$ and $\theta_{wd2}(log(s))$, the volumetric water content during drying θ_{wd} can be obtained:

$$\theta_{wd}(log(s)) = \int_{log(s^*)}^{log(s_{max})} G(log(s))d\,log(s) + \int_{log(s_{min})}^{log(s^*)} G(log(s))d\,log(s)\left(\frac{\int_{log(s^*)}^{log(s_{max})} G(log(s))d\,log(s)}{\int_{log(s_{min})}^{log(s_{max})} G(log(s))d\,log(s)}\right)^n \quad (26)$$

At a given suction s during the wetting process, the pores filled with water are those with a radius equal to or larger than the corresponding radius ($2T_s\,cos\,\theta/s$) minus the pores bounded by larger pores. The volumetric water content in the soil pores with a radius equal to or larger than the corresponding radius is expressed as $\int_{log(s^*)}^{log(s_{max})} G(log(s))d\,log(s)$. The volume fraction of pores bounded by larger pores c is

$$c = \left(\int_{log(s_{min})}^{log(s^*)} G(log(s))d\,log(s) / \int_{log(s_{min})}^{log(s_{max})} G(log(s))d\,log(s)\right)^n. \quad (27)$$

The volumetric water content during wetting θ_{ww} can be expresses as

$$\theta_{ww}(log(s)) = \int_{log(s^*)}^{log(s_{max})} G(log(s))d\,log(s)\,(1-c). \quad (28)$$

Thus, combining Equations (27) and (28) gives the volumetric water content during wetting θ_{ww}:

$$\theta_{ww}(log(s)) = \int_{log(s^*)}^{log(s_{max})} G(log(s))d\,log(s)\left[1 - \left(\frac{\int_{log(s_{min})}^{log(s^*)} G(log(s))d\,log(s)}{\int_{log(s_{min})}^{log(s_{max})} G(log(s))d\,log(s)}\right)^n\right] \quad (29)$$

In view of the above equations, the input parameters needed consist of one measured PSD curve at a given stress and suction, the initial void ratio e_0, two soil compressibility indices α_p and α_s, and the material parameter K. Table 1 summarises all of the parameters used in the comparisons reported in this paper.

Verification of the new model

Variation in the PSD under various stress paths

Simms and Yanful (2001) measured the PSD variation of London till before and after drying from

saturated conditions to a suction of 2500 kPa. Fig. 3 compares the measured and computed PSDs when drying to 2500 kPa. The initial PSD in the saturated state as one of the input parameters is also shown in this figure. The initial void ratio at saturated conditions is 0.47 and the plastic compressibility index λ_s is 0.05. The material parameter K is fitted to be 9.67. The scaling factor β and the shifting factor χ are determined to be 0.75 and 0.03, respectively, from Equations (13) and (14). The PSD at a suction of 2500 kPa is then predicted from Equation (3). As can be seen from the figure, when suction increases from 0 to 2500 kPa, the computed PSD matches the experimental data reasonably well. The slight difference is mainly due to the idealised method for describing the variation in the PSD, as shown in Fig. 2. In the idealized model, the overall shape of the PSD curve stays the same. However, the PSD of tested London till changes from bimodal to unimodal during the drying process, which cannot be captured by the idealised model. Hence, the computed pore volume density function in the pore with a radius ranging from 0.01 to 0.5 μm is smaller than the measured one at a suction of 2500 kPa.

Nowamooz and Masrouri (2010) measured the PSDs of a loose bentonite and silt mixture at an initial suction of 20 MPa and under saturated conditions. Fig. 4 compares the measured and computed PSDs when wetting from a suction of 20 to 0 MPa. The initial PSD at a suction of 20 MPa is shown in Fig. 4. The initial void ratio at a suction of 20 MPa is 0.8 and the plastic compressibility index λ_s of this swelling soil is 0.11. Following the same calculation procedure as that for London till, the PSD after wetting to a saturated state is predicted. The material parameter K, shifting factor χ, and scaling factor β are shown in Table 1. It can be seen that the computed PSD closely predicts the experimental data, which indicates that the above method can predict the shift of the PSD curve during not only the drying process but also the wetting process. Moreover, the predicted PSD of a loose bentonite and silt mixture after wetting shown in Fig. 4 is more accurate than that of London till after drying shown in Fig. 3. This is because during the wetting process from a suction of 20 MPa to saturation, the overall shape of the PSD of the loose bentonite and silt mixture does not change.

The PSDs of Kaolin clay before and after compression from 0 to 100 kPa at K0 conditions was measured by Yu et al. (2016). The measured and computed PSDs when compression to 100 kPa are compared in Fig. 5. One of the input parameters of the initial PSD before compression is also shown in Fig. 5. The initial void ratio before compression is 1.62. The plastic compression index λ_p is around

0.03. The calculation procedure is the same as that described above and the material parameter K, shifting factor χ, scaling factor β are also shown in Table 1. As can be seen from the figure, the predicted PSD curve after compression matches the measured data very well. This is because the shifting factor χ and scaling factor β can describe the variation in the PSD closely when the overall shape of the PSD does not change during mechanical loading. The comparisons between measured and computed data confirm that the proposed method to predict the variation in the PSD induced by hydro-mechanical loading is feasible and works well. In Fig. 5, the PSD evolution is insignificant because the decrease in the void ratio is just 4% during the compression process. With a larger change in density, the PSD evolution becomes more significant, as shown in Figs. 3 and 4. The change in the PSD can have an important effect on the WRC (Zhou and Ng, 2014).

Drying and wetting paths of the WRC

Zhang and Li (2010) measured the PSDs and WRCs of three types of soil: lean clay with sand (CL), sandy silt (ML) and clayey sand with gravel (SC). The measured WRC of a specimen of lean clay with sand is shown in Fig. 6. The initial void ratio before drying is 1.00 and the plastic compressibility index λ_s is 0.05. The material parameter K is equal to 11.07. The scaling factor β and shifting factor χ corresponding to the changing suction during the drying process can be calculated from Equations (13) and (14). Hence, at each suction value, a corresponding PSD curve can be obtained. Using Equation (15), each intrinsic PSD without influence of pore non-uniformity can be computed. Then the main drying path of the WRC, as shown in Fig. 6, can be calculated from Equation (19). As can be seen from the figure, the computed drying path of the WRC matches the measured one well. This is because the PSD variation with increasing suction during the drying process has been taken into consideration. Furthermore, using Equation (20), the wetting path of the WRC shown in Fig. 6 can be computed. Unlike previous models that predict the WRC directly from the PSD (Prapaharan et al., 1985; Zhang and Li, 2010; Sun et al., 2016), the wetting path of the WRC can be obtained in this study by considering the effects of pore non-uniformity on the water content.

Fig. 7 shows the measured WRC of a sandy silt specimen. The initial void ratio is 0.59 and the plastic compressibility index λ_s is 0.05. The material parameter K for this soil is fitted to be 1.52.

During drying, suction keeps increasing resulting in variations in both the scaling factor β and the shifting factor χ. A series of PSDs during the drying process can then be obtained from Equations (3), (13) and (14). Each corresponding intrinsic PSD without the influence of pore non-uniformity can be computed from Equation (15). The main drying path is predicted from the obtained intrinsic PSDs, as shown in Fig. 7. The computed drying path of the WRC, which takes into account the PSD variation, predicts the measured data reasonably accurately. Moreover, the wetting path computed by considering the PSD variation and the effects of pore non-uniformity is also shown in this figure.

Fig. 8 shows the measured WRC of a specimen of clayey sand with gravel. The initial void ratio is 0.53 and the plastic compressibility index λ_s is 0.05. The material parameter K for this type of soil is 15.03. During the drying process, the scaling factor β and the shifting factor χ can be calculated from Equations (13) and (14). The variation in the PSD during the drying path can then be modelled. A series of intrinsic PSDs without the influence of pore non-uniformity is computed with Equation (15) and used to predict the drying path of the WRC. The measured and computed drying paths of the WRC are shown in Fig. 8. The computed drying path of the WRC is good, but not as good as the predictions for the specimen of lean clay with sand and the sandy silt specimen. The measured and computed drying paths of the WRC do not completely agree possibly because the measured cumulative pore volume in the MIP test is smaller than the actual volume. MIP tests can only measure soil pores with a radius ranging from 10 nm to 400 μm. (Romero and Simms, 2008). For this clayey sand with gravel, some of the soil pores might have a radius falling outside this range (Zhang and Li, 2010). An incomplete PSD curve results in a difference between the measured and computed drying paths of the WRC. The predicted wetting path of the WRC is also shown in this figure.

Romero et al. (1999) measured the PSD curve and the drying-wetting cycle of the WRC of Boom clay. The initial void ratio is 0.59 and the plastic compressibility index λ_s is 0.07. The material parameter K is fitted to be 13.60. The scaling factor β and the shifting factor χ change with a change in suction and are calculated from Equations (13) and (14) respectively. After obtaining each PSD curve under a certain suction value during drying, the corresponding intrinsic PSDs without the influence of pore non-uniformity are computed from Equation (15). The drying path and wetting paths of the WRC are then obtained from Equations (19) and (20), respectively. Fig. 9 compares the measured and

computed drying and wetting paths of the WRC of the tested soil. As can be seen from the figure, the desorption rate and adsorption rate shown by the calculated drying path and wetting path are close to the measured data. The size of the hysteresis loop is also close to the measured data. However, the air entry value shown by the calculated drying path is about 15% lower than the measured one. This may be because the material parameter K used in the proposed model is assumed to be a constant. However, the shape factor describing different particle configurations in Equation (4) may change under hydro-mechanical loading, which may also influence the predicted results. The ability of the proposed model to predict the drying-wetting cycle of the WRC has only been somewhat verified in this study due to a lack of both the PSD and drying-wetting data of the same soil. More experimental work is needed on the PSD and drying-wetting cycle of the WRC to verify the proposed model more comprehensively. Moreover, hysteresis induced by the evolution of contact angle during drying and wetting should be considered.

Summary and conclusions

A new model is proposed to deduce the intrinsic PSD from the results of MIP tests, which are affected by pore non-uniformity. Moreover, the variation in the PSD under hydro-mechanical loads is incorporated in the model. The new model is applied to predict the change in PSDs during drying, wetting and compression. The computed PSDs match the experimental data well.

Based on the predicted PSDs at various levels of stress and suction, both the drying and wetting WRCs of unsaturated soil are calculated. Measured and computed WRCs of four different soils are compared and analysed. It is evident that the WRC can be well captured by the proposed model.

Acknowledgement

This work was supported by the National Natural Science Foundation of China (Grant No. 41572246, 41772280, 51509041), National Science Foundation of China for Excellent Young Scholars (Grant No. 41322019) and Research Grants Council of the Hong Kong Administrative Region (Grant No. 616812, 16209415).

References

Alonso EE, Gens A, Josa A (1990) A constitutive model for partially saturated soils. *Géotechnique* 40(3): 405–430

Burton GJ, Pineda JA, Sheng DC, Airey D (2015) Microstructural changes of an undisturbed, reconstituted and compacted high plasticity clay subjected to wetting and drying. *Engineering Geology* 193: 363-373

Dolinar B (2015). Prediction of the soil-water characteristic curve based on the specific surface area of fine-grained soils. *Bulletin of Engineering Geology and the Environment* 74(3): 697–703

Fredlund D, Xing A (1994) Equations for the soil-water characteristic curve. *Canadian Geotechnical Journal* 31(4): 521-532

Gao Y, Sun DA, Wu Y. (2018) Hysteretic soil water characteristics and cyclic swell–shrink paths of compacted expansive soils. *Bulletin of Engineering Geology and the Environment* 77:837–848

Hillel D (1998) Environmental soil physics. Academic Press, San Diego, CA, pp 155-161

Hu R, Chen YF, Liu HH, Zhou CB (2013) A water retention curve and unsaturated hydraulic conductivity model for deformable soils: consideration of the change in pore-size distribution. *Géotechnique* 63(16): 1389-1405

Li X, Zhan, LM (2009) Characterization of dual-structure pore-size distribution of soil. *Canadian Geotechnical Journal* 46(2): 129-141

Li ZS, Derfouf FE, Benchouk A, Abou-Bekr N, Taibi S, Fleureau JM (2018) Volume Change Behavior of Two Compacted Clayey Soils under Hydraulic and Mechanical Loadings. *Journal of Geotechnical and Geoenvironmental Engineering* 144(4): 04018013

Ng CWW, Lai CH, Chiu CF (2012) A modified triaxial apparatus for measuring the stress path-dependent water retention curve. *Geotechnical Testing Journal* 35(3): 490-495

Ng CWW, Menzies B (2007) Advanced unsaturated soil mechanics and engineering. Taylor & Francis, p. 687.

Ng CWW, Pang YW (2000) Influence of stress states on soil-water characteristics and slope stability. *Journal of Geotechnical and Geoenvironmental Engineering, ASCE* 126(2):157-166

Nowamooz H, Masrouri F (2010) Suction variations and soil fabric of swelling compacted soils. *Journal*

of Rock Mechanics and Geotechnical Engineering 2(2): 129-134

Penumadu D, Dean J (2000) Compressibility effect in evaluating the pore-size distribution of kaolin clay using mercury intrusion porosimetry. *Canadian Geotechnical Journal* 37(2): 393-405

Prapaharan S, Altschaeffl AG, Dempsey BJ (1985) Moisture curve of compacted clay: mercury intrusion method. *Journal of Geotechnical Engineering* 111(9): 1139-1143

Puppala AJ, Punthutaecha K, Vanapalli SK (2006) Soil-Water Characteristic Curves of Stabilized Expansive Soils. *Journal of Geotechnical and Geoenvironmental Engineering* 132(6): 736-751

Romero E, Gens A, Lloret A (1999) Water permeability, water retention and microstructure of unsaturated compacted Boom clay. *Engineering Geology* 54(1): 117-127

Romero E, Simms PH (2008) Microstructure investigation in unsaturated soils: a review with special attention to contribution of mercury intrusion porosimetry and environmental scanning electron microscopy. *Geotechnical and Geological Engineering* 26: 705-727

Romero E, Vecchia GD, Jommi C (2011) An insight into the water retention properties of compacted clayey soils. *Géotechnique* 61(4): 313-328

Santamarina JC, Jang J (2011) Bacteria in sediments: pore size effects. Géotechnique Letters 1: 91–93

Satyanaga A, Rahardjo H, Leong EC, Wang JY (2013) Water characteristic curve of soil with bimodal grain-size distribution. *Computers and Geotechnics* 48: 51-61

Simms PH, Yanful EK (2001) Measurement and estimation of pore shrinkage and pore distribution in a clayey till during soil-water characteristic curve tests. *Canadian Geotechnical Journal* 38(4): 741-754

Simms PH, Yanful EK (2002) Predicting soil-water characteristic curves of compacted plastic soils from measured pore-size distributions. *Géotechnique* 52(4): 269-278

Simms PH, Yanful EK (2005) A pore-network model for hydromechanical coupling in unsaturated compacted clayey soils. *Canadian Geotechnical Journal* 42(2): 499-514

Sun DA, Gao Y, Zhou AN, Sheng DC (2016) Soil-water retention curves and microstructures of undisturbed and compacted Guilin lateritic clay. *Bulletin of Engineering Geology and the Environment* 75(2): 781-791

Vanapalli SK, Fredlund DG, Puhafl DE (1999) The influence of soil structure and stress history on the soil-water characteristics of a compacted till. *Géotechnique* 49(2): 143-159

Yu CY, Chow JK, Wang YH (2016) Pore-size changes and responses of kaolinite with different structures subject to consolidation and shearing. *Engineering Geology* 202: 122-131

Zhang LM, Li X (2010) Microporosity structure of coarse granular soils. *Journal of Geotechnical and Geoenvironmental Engineering* 136(10): 1425-1436

Zhou C, Ng CWW (2014) A new and simple stress-dependent water retention model for unsaturated soil. *Computers and Geotechnics* 62: 216-222

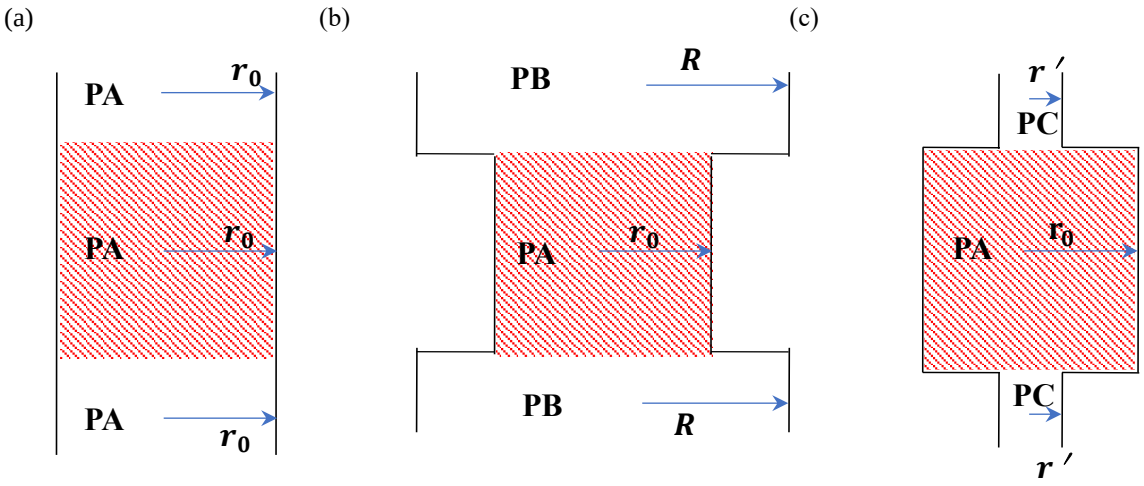

Fig. 1 Three idealised pore configurations: (a) a pore with a uniform radius; (b) a pore bounded by larger pores; and (c) a pore bounded by smaller pores

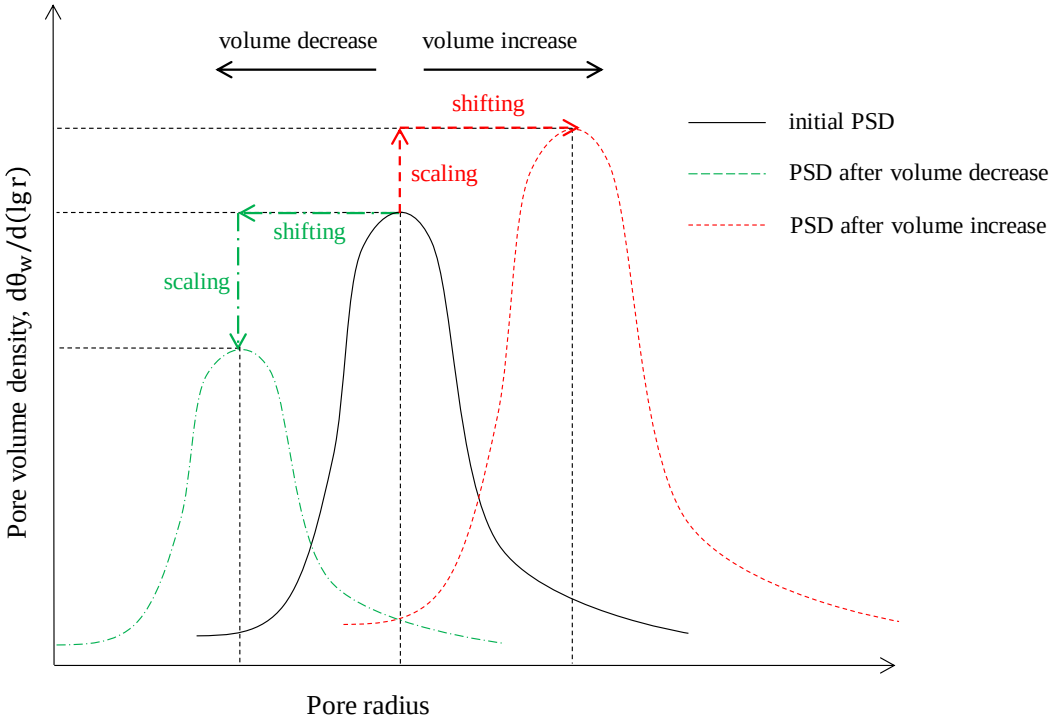

Fig. 2 Idealised model for describing shifts of the PSD curve

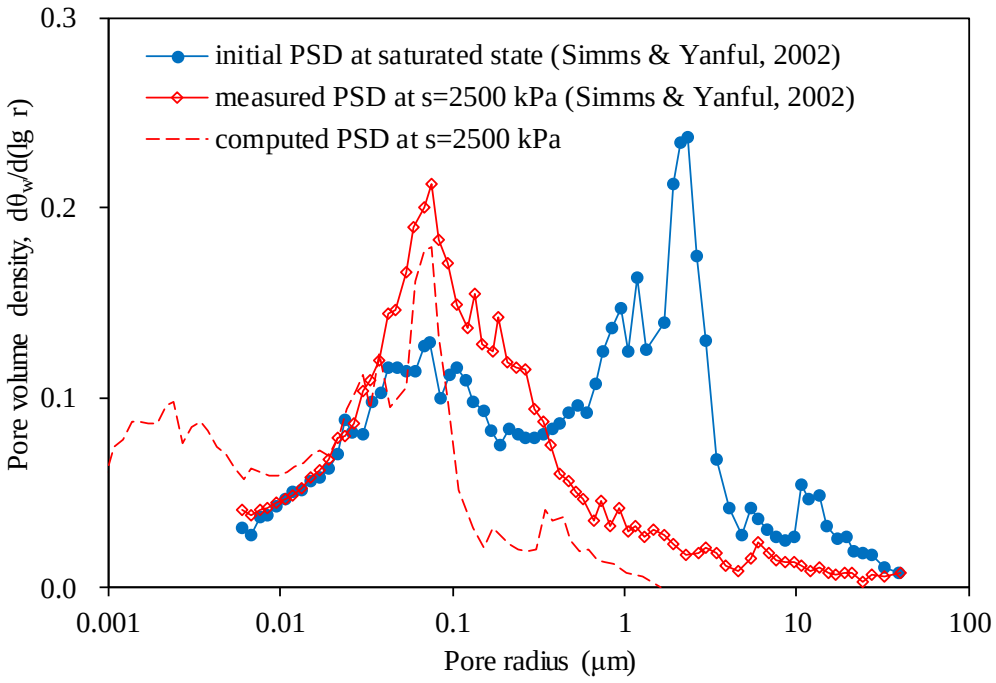

Fig. 3 Comparisons between the measured and computed PSD curves of London till: drying from a saturated state to a suction of 2500 kPa

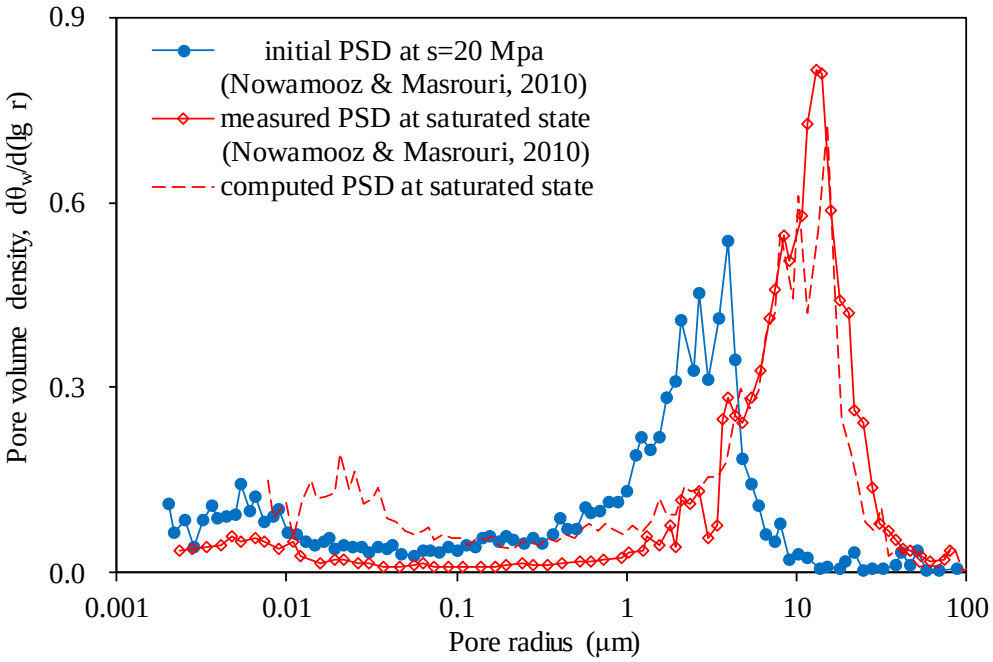

Fig. 4 Comparisons between the measured and computed PSD curves of a Bentonite and silt mixture: wetting from a suction of 20 MPa to a saturated state

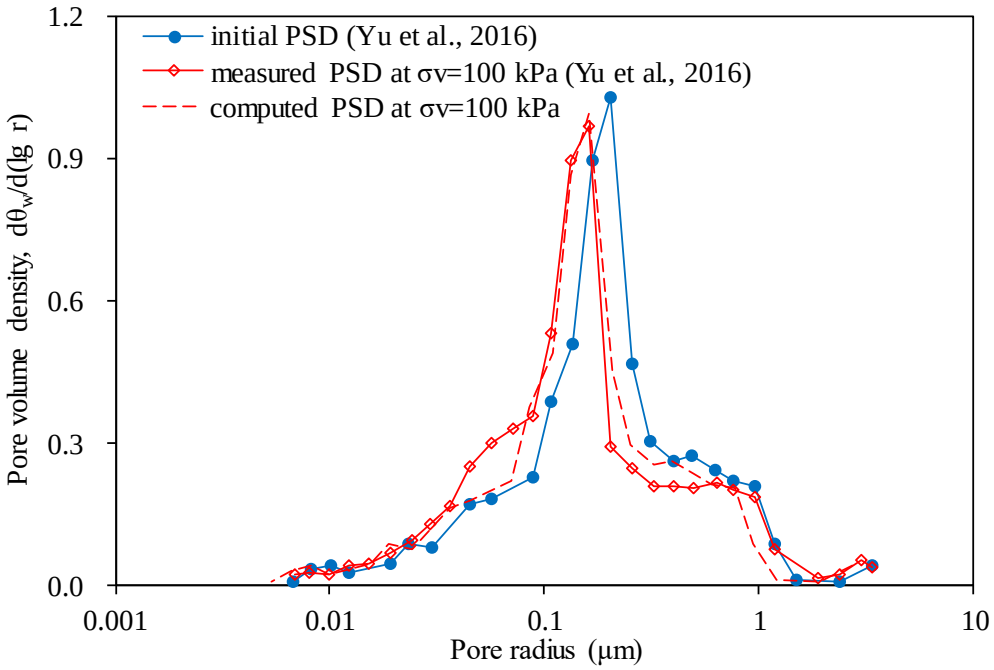

Fig. 5 Comparisons between the measured and computed PSD curves of Kaolin clay: compression from 0 to 100 kPa

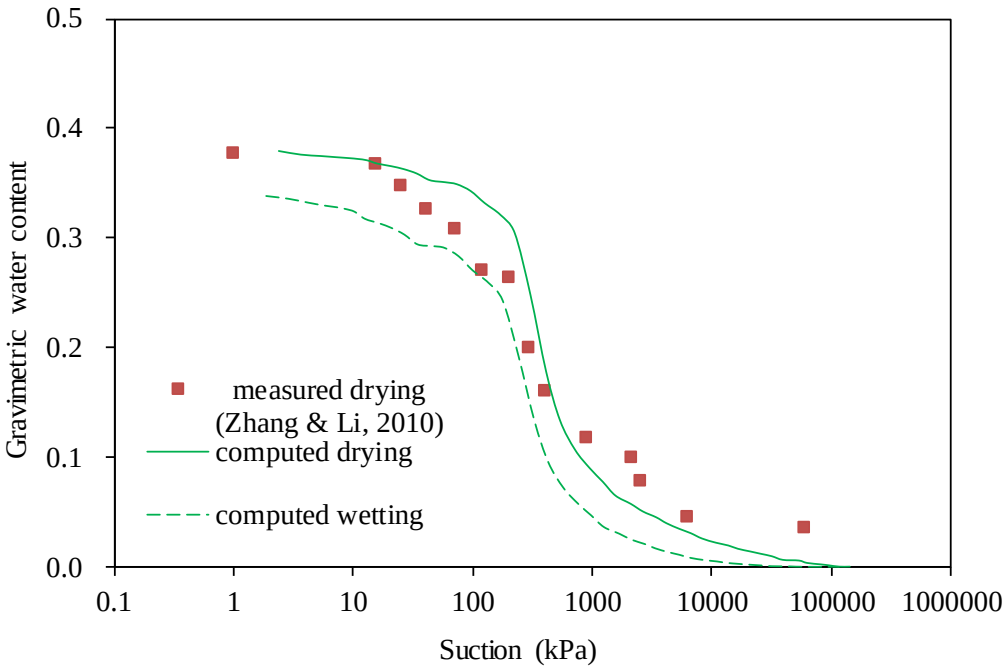

Fig. 6 Comparisons between the measured and computed WRCs of a lean clay with sand

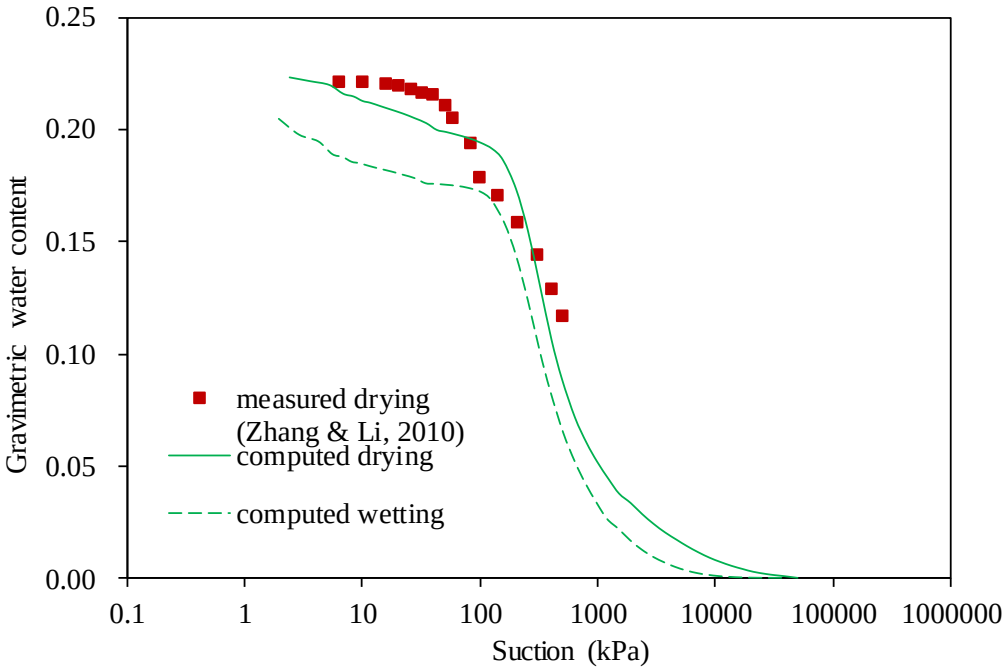

Fig. 7 Comparisons between the measured and computed WRCs of a sandy silt

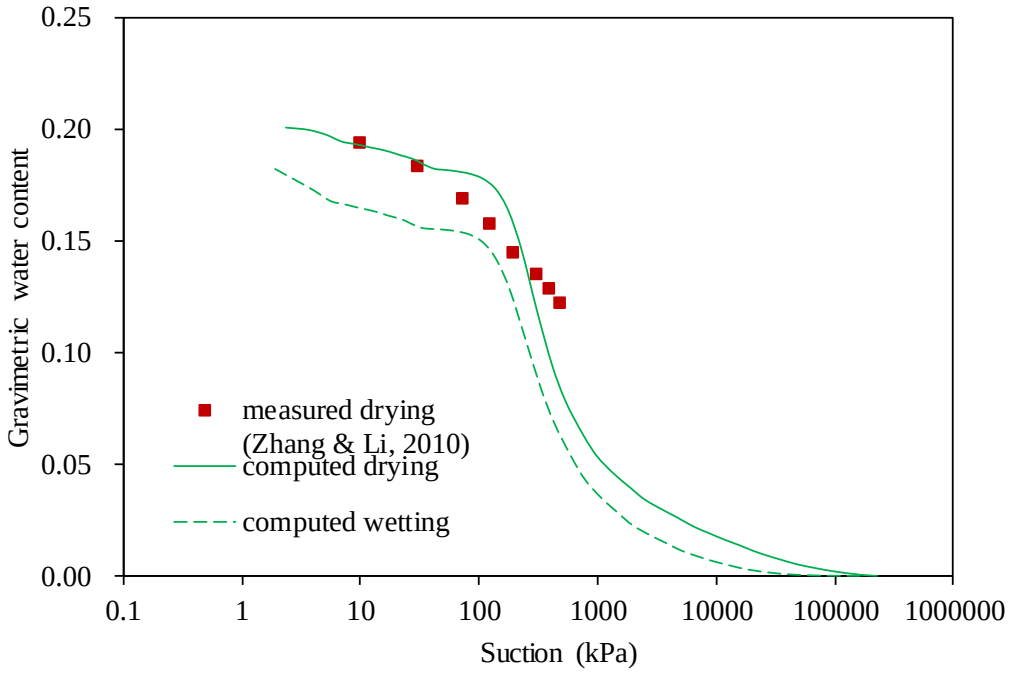

Fig. 8 Comparisons between the measured and computed WRCs of a clayey sand with gravel

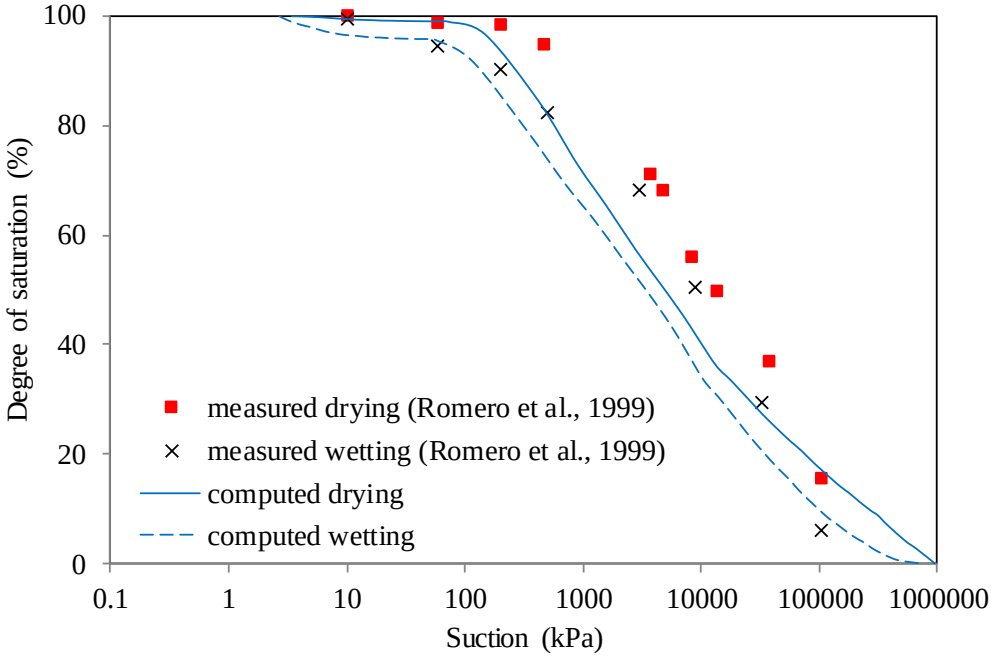

Fig. 9 Comparisons between the measured and computed WRCs of Boom clay

Table 1 Summary of input parameters

Soil classification	Stress path	Reference	e_0	α_p	α_s	K	Remarks
● Modelling variation in the PSD under hydro-mechanical loads							
Clayey gravel with sand (London till)	Drying from 0 to 2500 kPa	Simms and Yanful, 2002	0.47	-	0.05	9.67	β=0.75 χ=0.03 when drying from saturation to suction of 2500 kPa
Fat clay (Bentonite/ silt mixture)	Wetting from 20 MPa to 0	Nowamooz and Masrouri, 2010	0.80	-	0.11	0.84	β=0.74 χ=3.87 when wetting from suction of 20 MPa to saturation
Fat clay (Kaolinite)	Compression from 0 to 100 kPa	Yu et al., 2016	1.62	0.03	-	0.71	β=0.97 χ=0.80 when compression from 0 to 100 kPa
● Modelling hysteretic WRCs during drying and wetting							
Lean clay with sand	Drying path	Zhang and Li, 2010	1.00	-	0.05	11.07	β and χ changes during drying and wetting (See Equations (13) and (14)).
Sandy silt	Drying path	Zhang and Li, 2010	0.59	-	0.05	1.52	
Clayey sand with gravel	Drying path	Zhang and Li, 2010	0.53	-	0.05	15.03	
Fat clay (Boom clay)	Drying-wetting	Romero et al, 1999	0.59	-	0.05	13.60	

*Soil classification in this table is according to the Unified Soil Classification System (ASTM, 2011).